Eur. Phys. J. A **3**, 237–242 (1998)

THE EUROPEAN PHYSICAL JOURNAL A

Effective magnetic dipole operators for ^{88}Sr and ^{90}Zr closed-shell cores

I.P. Johnstone, I.S. Towner

Department of Physics, Queen's University, Kingston, Ontario K7L 3N6, Canada

Received: 31 May 1998
Communicated by W. Weise

Abstract. Core-polarisation and meson-exchange current calculations have been performed at ^{88}Sr and ^{90}Zr closed-shell cores to determine the effective magnetic dipole operator for valence orbitals. The values obtained show considerable core- and orbit-dependency. The results are tested in shell-model calculations for magnetic moments in N=50 and N=51 nuclides and the comparison with experiment is satisfactory.

PACS. 21.10.Ky Electromagnetic moments – 21.60.Cs Shell model – 27.60.+j $90 \leq A \leq 149$

1 Introduction

It is common practice in nuclear shell-model calculations to use effective operators when calculating electromagnetic moments and transition rates. Configurations lying outside the model space cause a renormalisation of the relevant operators, and this is taken into account by introducing parameters, which are either calculated or fitted to experimental data. Examples are the effective charges used for the electric quadrupole operator and effective g-factors used for the magnetic dipole operator.

In a recent paper[1] we calculated quadrupole effective charges for the region of mass A=90, and found significant differences between the values for ^{88}Sr and ^{90}Zr closed-shell cores. In the current paper we calculate g-factors for the same mass region and again find appreciable core dependency. The details of the calculated effective g-factors are given in Sect. 2. Two-body core-polarisation corrections are discussed in Sect. 3, and in Sect. 4 are used together with the calculated g-factors in shell-model calculations of N=50 and N=51 nuclei. In addition, a least-squared fit is carried out to determine best-fit values of the single-particle moments, to be compared with the calculated moments.

2 Calculation of effective g-factors

The magnetic moment operator in finite nuclei is modified from the free-nucleon operator due to core-polarisation and meson-exchange current (MEC) corrections[2,3]. The effective operator is defined as

$$\boldsymbol{\mu}_{\rm eff} = g_{l,\rm eff}\mathbf{l} + g_{s,\rm eff}\mathbf{s} + g_{p,\rm eff}[Y_2,\mathbf{s}], \qquad (1)$$

where $g_{x,\rm eff} = g_x + \delta g_x$, ($x = l$, s or p), with g_x the free-nucleon g-factor and δg_x the correction to it. The term $[Y_2,\mathbf{s}]$, which is absent from the free-nucleon operator, is a spherical tensor of multipolarity one formed by coupling a spherical harmonic of rank two to the spin operator. The free-nucleon values for g_l and g_s are 0 and −3.826 for neutrons, 1 and 5.587 for protons.

We here calculate in perturbation theory the corrections δg_x for closed-shell plus or minus one configurations relative to the closed shell ^{88}Sr (in which the proton $p_{1/2}$ orbital is empty) and ^{90}Zr (in which this orbital is filled). The three g-factors, δg_l, δg_s and δg_p, are determined by evaluating each of the one-body diagrams three times: (a) linking $j = l + 1/2$ with $j = l + 1/2$, (b) $j = l + 1/2$ with $j = l - 1/2$, and (c) $j = l - 1/2$ with $j = l - 1/2$. All the one-body graphs required for the evaluation of the core-polarisation correction are given in Figs. 1 - 4. In Fig. 1, diagram (a) is the zeroth-order term; it represents the free-nucleon operator evaluated between single-particle oscillator states. Diagrams (b) and (c) are the only first-order terms; they are the graphs originally evaluated by Arima and Horie[4], who showed they lead to a strong quenching of the spin g-factor, g_s. These graphs select out just the

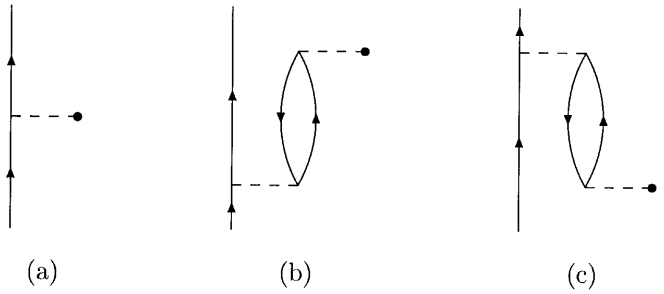

Fig. 1. Zeroth-order and first-order core-polarisation graphs. Diagram (c) is the Hermitian adjoint of diagram (b)

Table 1. Calculated effective g-factors and magnetic-moment corrections (in nuclear magnetons) for the $0g$ orbital in closed-shell-plus (or minus)-one configurations, broken down by class of diagram

	Proton				Neutron			
	δg_l	δg_s	δg_p	$\delta\mu(g_{9/2})$	δg_l	δg_s	δg_p	$\delta\mu(g_{9/2})$
				^{88}Sr core: $\pi p_{1/2}$-orbit empty				
CP-RPA:	0.011	−0.821	0.928	−0.299	−0.005	0.995	1.115	0.560
CP-RPA-vertex:	0.011	−0.457	0.334	−0.159	−0.005	0.481	−1.051	0.144
CP-NCS($\leq 6\hbar\omega$):	−0.136	−0.623	1.186	−0.768	0.133	0.188	0.864	0.687
CP-NCS($\geq 8\hbar\omega$):	−0.047	−0.324	−0.008	−0.349	0.044	0.209	0.023	0.282
MEC:	0.145	0.411	−0.536	0.745	−0.108	−0.193	0.292	−0.507
Isobars:	−0.003	−0.360	0.754	−0.137	0.002	0.360	−0.796	0.132
Relativistic:	−0.027	−0.167	−0.045	−0.193	0.000	0.102	0.000	0.051
CP-MEC:	0.110	0.262	0.575	0.613	−0.106	−0.241	−0.597	−0.587
Sum:	0.065	−2.078	3.187	−0.548	−0.045	1.901	−0.150	0.761
				^{90}Zr core: $\pi p_{1/2}$-orbit full				
CP-RPA:	0.011	−0.347	−0.071	−0.133	0.001	0.761	0.232	0.399
CP-RPA-vertex:	0.009	−0.209	0.135	−0.057	−0.004	0.336	−0.175	0.140
CP-NCS($\leq 6\hbar\omega$):	−0.138	−0.639	1.196	−0.787	0.150	0.233	1.446	0.822
CP-NCS($\geq 8\hbar\omega$):	−0.047	−0.324	−0.008	−0.349	0.044	0.209	0.023	0.282
MEC:	0.145	0.410	−0.525	0.747	−0.114	−0.195	0.259	−0.535
Isobars:	−0.003	−0.367	0.793	−0.137	0.002	0.367	−0.802	0.134
Relativistic:	−0.027	−0.167	−0.045	−0.193	0.000	0.102	0.000	0.051
CP-MEC:	0.110	0.262	0.575	0.613	−0.106	−0.241	−0.597	−0.587
Sum:	0.061	−1.379	2.051	−0.297	−0.027	1.572	0.386	0.706

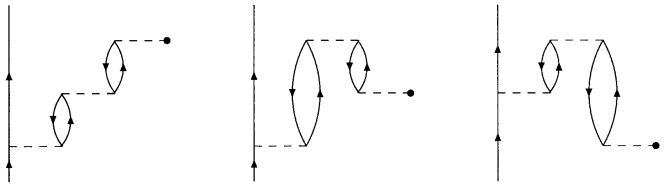

Fig. 2. Second-order graphs contributing to the RPA series. Hermitian adjoint graphs are not shown

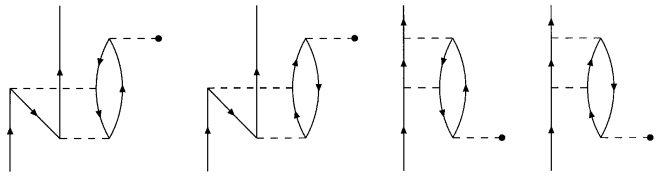

Fig. 3. Second-order graphs representing vertex corrections to the RPA series. Hermitian adjoint graphs are not shown

1^+ particle-hole components in the residual interaction; for a ^{90}Zr closed-shell core there is only one such component, namely neutron $(g_{9/2}^{-1}, g_{7/2})$. For a ^{88}Sr closed shell there is a second 1^+ particle-hole state involving p-orbits, namely proton $(p_{3/2}^{-1}, p_{1/2})$.

In Fig. 2 some second-order graphs involving 1^+ particle-hole intermediate states are shown. These graphs represent a start of a geometrical series, which we sum to all orders. This is equivalent to a Random Phase Approximation (RPA) calculation. The second-order graphs are out of phase with the first-order graphs, so the series alternates in sign. The results of the summation is given in Table 1, where it is labelled CP-RPA. We show the results for a proton and a neutron in a $0g$ orbit for the cases of ^{88}Sr and ^{90}Zr closed-shell cores. The residual interaction in these calculations is taken as a one-boson-exchange potential multiplied by a short-range correlation function. This modification is an approximate, but easy, way to obtain a G-matrix. The potential is of the Bonn type[6], with the values of the meson masses and coupling constants given in[2]. It is important to use here a one-boson-exchange potential as the residual interaction so that the meson-exchange current operators, to be discussed shortly, can be constructed consistently with the same meson masses and coupling constants.

Note the RPA correction mainly quenches the g_s value. For protons there is a big reduction in the quenching in moving from a ^{88}Sr to a ^{90}Zr core due to the removal of the proton $(p_{3/2}^{-1}, p_{1/2})$ particle-hole state from the calculation. There is also a reduction for neutrons, but not quite so large. From Fig. 2 one can see that the valence particle is not antisymmetrised with respect to the particle line in the second bubble. This is corrected by the series of diagrams shown in Fig. 3, which are known as the RPA vertex-correction graphs. Their contribution is in phase with the RPA calculation increasing the quenching of g_s. This contribution is labelled in Table 1 as CP-RPA-vertex.

In Fig. 4 are a number of diagrams in which the one-body operator acts on a particle or hole line as opposed to operating on a particle-hole pair. This set of diagrams is called a 'number-conserving' set (NCS). That is, if the

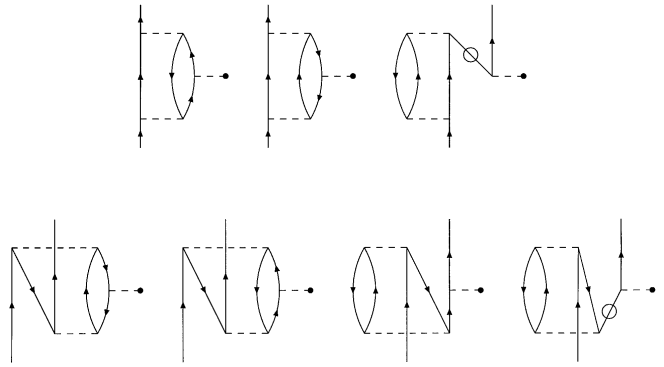

Fig. 4. Second-order graphs representing the number-conserving sets. Lines with a 'loop' on them are folded lines [5] and represent normalisation-correction graphs. Hermitian adjoint graphs are not shown

Table 2. Single-particle energies for neutrons and protons near the Fermi surface from pick-up and stripping reaction data. All other single-particle energies are given by $N\hbar\omega$ plus a spin-orbit shift from Eq. (2) and normalised to the $1d_{5/2}$ value for neutrons and to the $1p_{1/2}$ value for protons

	Neutron	Proton
$1p_{3/2}$	−15.14	−10.61
$0f_{5/2}$	−14.98	−11.03
$1p_{1/2}$	−11.50	−7.12
$0g_{9/2}$	−11.11	−6.25
$1d_{5/2}$	−6.36	−2.38
$2s_{1/2}$	−5.33	−0.47
$1d_{3/2}$	−4.35	−0.39
$0g_{7/2}$	−3.69	−0.69

magnetic moment operator is replaced by the number operator, the sum of these graphs would be identically zero. These graphs are difficult to compute because there are no selection rules to limit the number of intermediate states to be summed. We were able to sum these graphs up to intermediate-state energies of $6\hbar\omega$ above the energy of the valence nucleon in an oscillator basis. However it was evident that the calculation had not converged at this energy. We therefore proceeded with an approximate calculation. The closed shell is taken to be an LS closed shell, with A=80, and the computation performed in LS coupling. This leads to a great saving in computation time and makes the calculation tractable. However, the neutron-excess orbitals are not now treated correctly. The intermediate-state summation is explicitly computed up to $14\hbar\omega$ and geometrically extrapolated beyond that. We checked that an LS-coupling calculation for intermediate-state energies of $6\hbar\omega$ was in reasonable accord with the correct jj-coupling calculation for the same intermediate states. The results are shown separately for low- and high-energy intermediate states in Table 1, where they are labelled CP-NCS. It is seen these graphs are responsible for a large correction to the magnetic moments. For the spin part of the operator they are in phase with the RPA and provide more quenching to g_s. Additionally they give significant contributions to g_l, positive for neutrons and negative for protons.

Figs. 1 - 4 display all the core-polarisation graphs that contribute up to second order to the renormalisation of the magnetic moment operator. However we need to comment on the appropriate energy denominators to be used for the intermediate states in the perturbation expansion. Formally, these energies are given in terms of the eigenenergies of the single-particle states of the one-body Hamiltonian, the harmonic oscillator, and so are integral multiples of $\hbar\omega$. For the high-lying intermediate states, this is what we have used. However, as the closed-shell cores we are using for these calculations, ^{88}Sr and ^{90}Zr, are jj-closed shells rather than LS-closed shells, we cannot use simple integral multiples of $\hbar\omega$ for the single-particle energies of the low-lying states. This is because some of the unoccupied particle orbitals are degenerate with some of the occupied hole orbitals and that could result in certain energy denominators in the perturbation expansion becoming zero. Of course, it is the spin-orbit force that splits this degeneracy and in medium-mass nuclei the contribution of the spin-orbit force to level spacing is very important. Therefore, following Bohr and Mottelson[7], we add to the one-body oscillator the terms

$$v_{ls}\hbar\omega(\mathbf{l}.\mathbf{s}) + v_{ll}\hbar\omega\left(\mathbf{l}^2 - \langle\mathbf{l}^2\rangle_N\right), \tag{2}$$

$$\langle\mathbf{l}^2\rangle_N = \frac{1}{2}N(N+3), \tag{3}$$

where $N = 2n+l$ is the principal quantum number for the oscillator orbital, n the number of radial nodes (excluding the origin and infinity) and l the orbital angular momentum quantum number. There is no radial dependence to these terms, so the eigenfunctions remain oscillator functions, but the degeneracy among the single-particle energies is removed. We use the values $v_{ls} = -0.127$ and $v_{ll} = -0.03$ from[7]. We make a further fine adjustment to these energies for the single-particle states close to the Fermi surface so that they match exactly experimental values determined in pickup and stripping reactions. The values of the single-particle energies used are given in Table 2.

The other major ingredient to the renormalisation of the magnetic moment operator comes from meson-exchange currents (MEC). These MEC corrections arise because nucleons in nuclei are interacting through the exchange of mesons, which can be disturbed by the electromagnetic field. Since meson exchange involves two nucleons, the correction leads to two-body magnetic moment operators. In a closed-shell-plus-or-minus-one configuration, computation of this correction requires evaluation of the two-body matrix elements between the valence nucleon and one of the core nucleons, summed over all nucleons in the core. The results can be expressed in terms of an equivalent effective one-body operator, Eq. (1), acting on the valence nucleon alone. The details of the two-body MEC operators are described in[2] and updated in[8]. For consistency, the same mesons, coupling constants, masses and short-range correlations are used

in the construction of the MEC operators as are used in the one-boson-exchange potential. From Table 1, it is seen that the MEC correction is opposite sign to the CP-NCS correction and cancels a large part of it.

There are two further terms to consider. First is a mesonic correction in which the meson prompts the nucleon to be raised to an excited state, the Δ-isobar resonance, which is then de-excited by the electromagnetic field. This correction leads to a two-body operator that is handled like the MEC correction. Second is a relativistic correction to the one-body operator,[2]. Both these corrections amount to only a few percent change to the magnetic moment, but are retained for completeness.

Finally a further correction of the same order in meson-nucleon couplings is a core-polarisation correction to the two-body MEC operator. This term also suffers from an unrestricted summation over intermediate states, so we have only computed it approximately using LS coupling. Fortunately, as Arima *et al.*[9,10] have pointed out, the latter terms largely cancel the former. This correction is listed in Table 1 as CP-MEC and again it is seen to be of opposite sign to the CP-NCS correction and, together with the MEC correction, overpowers it. It is clear with so much cancellation involved the final results will be somewhat sensitive to the assumptions and approximations made here.

In Table 3 we gather together all these contributions to the renormalisation and give the summed result for all the orbitals involved in the shell-model calculations that follow. All matrix elements have been evaluated with harmonic oscillator radial functions of characteristic frequency $\hbar\omega = 9.08$ MeV. Note that with a term $[Y_2, \mathbf{s}]$, in the effective magnetic moment operator, Eq. (1), there are non-zero off-diagonal matrix elements between $0g_{7/2}$-$1d_{5/2}$ and $1d_{3/2}$-$2s_{1/2}$ orbitals. These l-forbidden matrix elements are zero with the free-nucleon operator but non-zero here. However, their impact in the present calculation is very small.

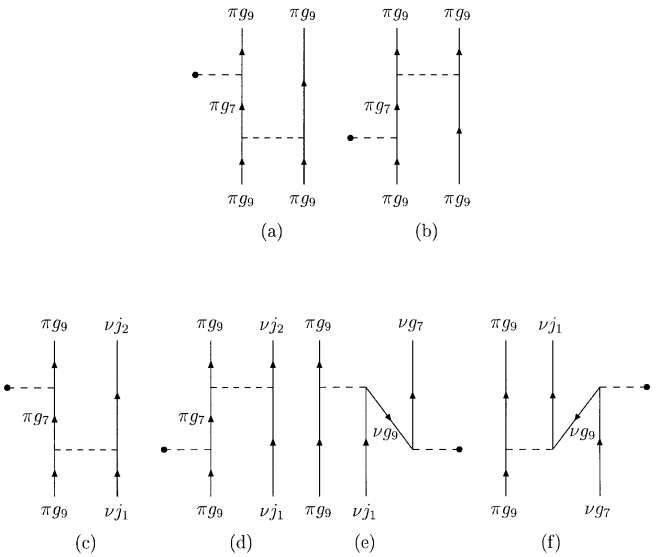

Fig. 5. First-order two-body core-polarisation graphs. The upper two diagrams involving only protons in the $g_{9/2}$ orbital are the only ones operative for N=50 nuclides. The lower four diagrams involving a proton-neutron interaction are additionally operative for N=51 nuclides. The neutron orbital, j_1 or j_2, may be either the $d_{5/2}$, $s_{1/2}$, $d_{3/2}$ or $g_{7/2}$ orbitals

3 Two-body corrections

The g-factor renormalisations, as calculated in Sect. 2, strictly apply only in closed-shells-plus-or-minus-one nucleon situations. Yet in the shell-model calculations, we will use these renormalised g-factors in closed-shell-plus-n cases, where is n is a small number representing the proton occupancy in the $g_{9/2}$ orbital. Whenever n is greater than 1, there are additional contributions to the core polarisation coming from interactions among the valence nucleons. Evaluating these contributions to just first order in perturbation theory leads to two-body diagrams. The appropriate first-order diagrams for N=50 and N=51 nuclei are given in Fig. 5. Diagrams (a) to (d) involve excitation of a $g_{9/2}$ proton into the $g_{7/2}$ shell, caused by interaction with either a proton or a neutron. Diagrams (e) and (f), which are of lesser importance due to the small $g_{7/2}$ components in N=51 wavefunctions, involve excitation of a $g_{9/2}$ neutron into the $g_{7/2}$ shell.

We have evaluated these diagrams with the one-boson exchange potential used for the core-polarisation calculations in Sect. 2 and with the proton and neutron single-particle energy gaps between the $g_{7/2}$ and $g_{9/2}$ orbitals set at 5.56 and 7.42 MeV respectively from Table 2. The $g_{9/2} \rightarrow g_{7/2}$ reduced matrix element required in the evaluation of the two-body diagrams was set equal to the value given by the g-factors of Table 3; doing this, rather than using free-nucleon g-factors, should effectively take into account higher-order diagrams. The result is a set of two-body matrix elements, which can be used in calculations of magnetic moments.

4 Shell-model calculations

The g-factors in Table 3 and two-body matrix elements from Sect. 3 were used in calculations of magnetic moments of N=50 and N=51 nuclei. Even-parity N=50 moments were calculated allowing $Z-38$ protons to occupy the $p_{1/2}$ and $g_{9/2}$ orbitals, making use of the JS1 interaction of Johnstone and Skouras[11]. Even-parity N=51 moments were calculated allowing the 51^{st} neutron to occupy the $d_{5/2}$, $s_{1/2}$, $d_{3/2}$ and $g_{7/2}$ orbitals, with protons again spanning the $p_{1/2}$ and $g_{9/2}$ shells. The interaction used was the JS4 interaction of Johnstone and Skouras[11]. The wavefunctions have components with the proton $p_{1/2}$ orbital filled and with the proton $p_{1/2}$ orbital empty, and for these different g-factors were used – namely, the values for ^{90}Zr and ^{88}Sr cores given in Table 3. Results of the calculations are given in Table 4.

Least chi-squared fits were carried out to determine best-fit values of effective $g_{9/2}$ and $d_{5/2}$ magnetic mo-

Table 3. Effective g-factors and magnetic moment corrections (in nuclear magnetons) from core-polarisation and MEC calculations. Here $\mu_{\rm sp}$ is the free-nucleon, single-particle value of the magnetic moment and $\mu_{\rm eff} = \mu_{\rm sp} + \delta\mu$

Orbital	δg_l	δg_s	δg_p	$j = l + 1/2$			$j = l - 1/2$		
				$\delta\mu$	$\mu_{\rm eff}$	$\frac{\mu_{\rm eff}}{\mu_{\rm sp}}$	$\delta\mu$	$\mu_{\rm eff}$	$\frac{\mu_{\rm eff}}{\mu_{\rm sp}}$
^{88}Sr core: $\pi p_{1/2}$-orbit empty									
π $1p$	−0.162	−2.506	1.315	−1.363	2.431	64%	0.135	−0.130	49%
π $0g$	0.065	−2.078	3.187	−0.548	6.246	92%	0.708	2.424	141%
ν $0g$	−0.045	1.901	−0.150	0.761	−1.152	60%	−0.896	0.592	40%
ν $1d$	−0.060	2.084	−1.469	0.838	−1.075	56%	−0.557	0.590	51%
ν $2s$		2.120		1.060	−0.853	45%			
ν $0g$-$1d$			−1.660						
ν $1d$-$2s$			−1.390						
^{90}Zr core: $\pi p_{1/2}$-orbit full									
π $1p$	0.086	−1.531	1.164	−0.633	3.160	83%	0.158	−0.107	40%
π $0g$	0.061	−1.379	2.051	−0.297	6.496	96%	0.546	2.262	132%
ν $0g$	−0.027	1.572	0.386	0.706	−1.207	63%	−0.759	0.729	49%
ν $1d$	−0.054	1.666	−1.404	0.644	−1.269	66%	−0.429	0.719	63%
ν $2s$		1.636		0.818	−1.095	57%			
ν $0g$-$1d$			−2.942						
ν $1d$-$2s$			−1.924						

Table 4. Magnetic moments (in nuclear magneton units) for nuclei with N=50 and N=51 calculated in the shell model (a) with the free-nucleon g-factors (Bare), (b) with the calculated effective g-factors from Table 3 plus the two-body core-polarisation diagrams (Calc), (c) with the chi-squared fits for the effective g-factors (Fit), compared with experimental values [12]

	Bare	Calc	Fit	Expt
^{90}Zr(8^+)	12.08	11.04	10.81	10.85 ± 0.06
^{91}Nb($21/2^+$)	15.85	14.38	14.06	12.4 ± 1.9
^{92}Mo(8^+)	12.08	11.32	11.24	11.31 ± 0.04
^{93}Tc($9/2^+$)	6.79	6.29	6.23	6.30 ± 0.05[a]
^{94}Ru(6^+)	9.06	8.32	8.27	8.12 ± 0.04
^{94}Ru(8^+)	12.08	11.11	11.03	11.10 ± 0.04
^{96}Pd(8^+)	12.08	10.90	10.84	10.97 ± 0.06
^{91}Zr($5/2^+$)	−1.84	−1.11	−1.35	-1.304 ± 0.000
^{91}Zr($21/2^+$)	10.17	9.98	9.87	9.82 ± 0.08
^{92}Nb(2^+)	6.65	5.93	6.09	6.137 ± 0.004
^{93}Mo($21/2^+$)	10.19	10.15	9.67	9.93 ± 0.08
^{94}Tc(7^+)	5.11	5.36	4.97	5.07 ± 0.07
^{95}Ru($5/2^+$)	−1.51	−0.74	−1.06	-0.861 ± 0.007[b]
^{95}Ru($17/2^+$)	7.53	7.52	7.07	7.01 ± 0.14[c]
^{95}Ru($21/2^+$)	10.32	10.12	9.64	9.17 ± 0.07

[a] Ref.[13], averaged with previous data [12]
[b] Ref.[14]
[c] Ref.[15]

ments. Chi squared is defined as

$$\chi^2 = \sum_i \left(\mu_i(\text{calc}) - \mu_i\right)^2 / (N\sigma_i^2), \qquad (4)$$

where the i^{th} experimental magnetic moment is μ_i, the corresponding uncertainty is σ_i, and N is the number of moments included in the fit. In order that the fit is not overly weighted by data with very small experimental uncertainties, we set the minimum uncertainty equal to the value required to give χ equal to unity. This, in effect, gives each experimental datum (with the exception of ^{91}Nb($21/2^+$)) an equal weight in the fit. Our estimate of the error in the effective moment, $\mu_{\rm eff}$, is then given by

$$\sigma_\mu^2 = \sum_i \left(\partial\mu_{\rm eff}/\partial\mu_i\right)^2 \left(\mu_i(\text{calc}) - \mu_i\right)^2. \qquad (5)$$

The fit was made to fifteen N=50 and N=51 even-parity moments, with the calculated two-body corrections and the small neutron contribution from other than diagonal $d_{5/2}$ matrix elements subtracted from the experimental values. This latter contribution was calculated using the g-factors of Table 3. The result was to give effective proton $g_{9/2}$ magnetic moments of $\mu_{\rm eff}(g_{9/2}) = 6.47 \pm 0.04\mu_N$ and $6.11 \pm 0.03\mu_N$, and effective neutron $d_{5/2}$ magnetic moments of $\mu_{\rm eff}(d_{5/2}) = -1.78 \pm 0.13\mu_N$ and $-0.94 \pm 0.08\mu_N$, when the proton $p_{1/2}$ orbital is filled and empty respectively. These are 95±0.7%, 90±0.5%, 93±7% and 49±4% of the free-nucleon values, whereas the calculations of Sect. 2 gave 96%, 92%, 66% and 55%. Agreement is good for three of the four cases. However for a $d_{5/2}$ neutron outside a ^{90}Zr core, the calculations are giving a larger renormalisation than appears to be evident in the fits to data.

The proton $p_{1/2}$ $\mu_{\rm eff}$ value can be determined from the magnetic moment of ^{89}Y($1/2^-$), which is known to very high precision. Assuming that this state is purely a $p_{1/2}$ particle outside the ^{88}Sr core, the $\mu_{\rm eff}$ is −0.137, only 52% of the single-particle value. This is in good agreement with the calculated value in Table 3 for ^{88}Sr plus particle, which is 49%. The calculated value, on the other hand, for a ^{90}Zr core minus a $p_{1/2}$ proton is only 40%. In principle, identical results should be obtained for both

cores, but in practice, our calculations do not quite satisfy this requirement. This is because the RPA series, as mentioned earlier, does not respect the antisymmetry of a particle line in the particle-hole bubble and the external valence particle line. This is corrected to second order by the CP-RPA-vertex graphs, but not to all orders.

5 Summary

We have calculated effective g-factors for nucleons in the region of mass A=90, by summing first- and second-order diagrams, including effects of meson-exchange currents. It is found that there are significant differences between g-factors calculated with a ^{88}Sr closed-shell core, in which the proton $p_{1/2}$ orbital is empty, and with a ^{90}Zr core, in which this shell is filled. Two-body core-polarisation corrections to magnetic moments have also been considered by evaluating appropriate first-order diagrams. The calculated one- and two-body operators have then been used in calculations of magnetic moments of N=50 and N=51 nuclei, and agreement with experiment is satisfactory.

In addition, we have tried to determine empirically the effective g-factors of the proton $g_{9/2}$ and neutron $d_{5/2}$ orbitals by performing least-square fits of shell-model calculations with four parameters to fifteen experimental data. For three of the four effective g-factors determined in this way there is a good correspondence with the theoretically calculated values. For the fourth case, a $d_{5/2}$ neutron orbital outside a ^{90}Zr closed shell, there is a big difference. Indeed, the empirical values of $\mu_{\rm eff}(d_{5/2}) = -1.78 \pm 0.13\mu_N$ and $-0.94 \pm 0.08\mu_N$ for cores of ^{90}Zr and ^{88}Sr respectively show a very large core dependency, much larger than the theoretical calculations indicate. Curiously, in a similar study[1] of effective charges for electric quadrupole moments the empirically determined values for a $d_{5/2}$ neutron also showed more dependency on the cores than theory anticipated. We have no explanation for this, but speculate that for N=51 isotones the shell-model space should be enlarged, possibly to include the neutron $h_{11/2}$ orbital.

References

1. I.P. Johnstone, I.S. Towner, Eur. Phys. J. **A2**, 263 (1998)
2. I.S. Towner, Phys. Reports **185**, 263 (1987)
3. B. Castel, I.S. Towner, *Modern Theories of Nuclear Moments,* (Clarendon, Oxford 1990)
4. A. Arima, H. Horie, Prog. Theor. Phys. **11**, 504 (1954); A. Arima, H. Horie, Prog. Theor. Phys. **12**, 623 (1954)
5. B.H. Brandow, Rev. Mod. Phys. **39**, 771 (1967)
6. R. Machleidt, Adv. Nucl.Phys. **19**, 189 (1989); R. Machleidt, K. Holinde, Ch. Elster, Phys. Reports **149**, 1 (1987)
7. A. Bohr, B.R. Mottelson, *Nuclear structure,* Vol. 2. (Benjamin, New York 1975)
8. I.S. Towner, in *Proc. of Int. Symp. on Non-nucleonic Degrees of Freedom Detected in Nucleus, Osaka, Japan, 1996,* edited by T. Minamisono, Y. Nojiri, T. Sato, K. Matsuta (World-Scientific, Singapore 1997), pp. 33-42
9. A. Arima, H. Hyuga, in *Mesons in Nuclei,* edited by D.H. Wilkinson, M. Rho, (North-Holland, Amsterdam 1979), p. 685
10. H. Hyuga, A. Arima, K. Shimizu, Nucl. Phys. **A336**, 363 (1981)
11. I.P. Johnstone, L.D. Skouras, Phys. Rev. **C51**, 2817 (1995)
12. P. Raghavan, Atomic Data and Nuclear Data Tables, **42**, 189 (1989)
13. B. Hinfurtner, E. Hagn, E. Zech, W. Troger, T. Butz, Z. Phys. **A350**, 311 (1995)
14. B. Hinfurtner, E. Hagn, E. Zech, Nucl. Phys. **A534**, 339 (1991)
15. A.I. Levon, O.F. Nemets, E.G. Mikhailov, V.P. Chepak, Bull. Acad. Sci. USSR, Phys. Ser. **40**, No. 6, 128 (1976)